Arch. Metall. Mater. **69** (2024), 2, 467-470

DOI: https://doi.org/10.24425/amm.2024.149768

DONG WAN LEE[1], JIN WOO KIM[1], SU GWAN LEE[1], DHIN VAN CONG[1],
JIN CHUN KIM[1*], HWI JUN KIM[2], JOONG GYEONG LIM[3], TAE SIK YOON[3]

MICROSTRUCTURAL CHARACTERISTICS OF MODIFIED ODS Ni-BASED SUPERALLOYS FABRICATED USING LASER-POWDER BED FUSION

Oxide dispersion-strengthened (ODS) superalloys are usually manufactured by a hot isostatic pressing after mechanical alloying (MA-HIP). However, this process cannot produce complex-shaped parts. Here, we used an additive manufacturing product (powders produced by laser powder bed fusion, L-PBF) to address this issue. Modified ODS Ni-based superalloy powders with a similar composition to the mechanical alloy 6000 (MA6000) were manufactured using a gas atomization process. The obtained powders and L-PBF synthesized samples were analyzed by scanning electron microscopy (SEM), X-ray diffraction (XRD), LPSA, and EBSD analyses.

Keywords: L-PBF; MA6000; ODS Ni-based superalloy; AM; microstructure

1. Introduction

Oxide dispersion-strengthened (ODS) Ni-based superalloys are widely used in the power, defense, space, and aviation industries. Demand for high-strength and high-temperature ODS Ni-based superalloys is rapidly increasing due to the desire to achieve energy efficiency in these industries [1].

Nano-oxide dispersion technologies to produce Ni-based superalloy materials have been under development for more than 40 years. Among them, the MA-HIP process is widely used. However, the long mechanical alloying process, low productivity of the HIP process, difficulty in manufacturing complex-shaped parts, and high manufacturing cost have limited application of the MA-HIP process [2,3].

In this study, modified ODS Ni-based superalloy powders with a composition similar to mechanical alloy 6000 (MA6000) were prepared using a plasma gas hybrid atomization (PGHA) process. We changed the alloy compositions and contents of yttrium oxide (Y_2O_3) and further treated the produced powders by the L-PBF process [4]. Densification and microstructural evolution were analyzed according to powder size and the L-PBF process [5].

2. Experimental

Powders were produced by the PGHA process (Daishinkangup Co., Ltd, Korea Rep). Ni-based superalloy powders with diameters <25 μm (powder #1), 25-45 μm (powder #2), and 45-60 μm (powder #3) were synthesized. Powder size and distribution were analyzed by Laser particle size analysis (LPSA). Powder shape was analyzed through scanning electron microscopy (SEM). EDS-XRF analyses were performed to confirm the composition of the as-prepared ODS Ni-based superalloy powders.

Powders #2 and #3 were used for L-PBF, while powder #1 was excluded due to powder application problems. An L-PBF machine (Metal3D-MetalSys120D, Korea Rep.) was used to manufacture four different samples (A1, A2, B1, B2), two of each powder size (#2 and #3), using the laser conditions described in TABLE 1.

The microstructure of the L-PBF-produced 3D samples was analyzed using SEM (JEOL-IT200, Japan). Three-dimensional samples were polished with #400 to #2000 sandpaper and then finely polished with 1 μm alumina powder suspension. Etching was performed using HCl-glycerol-HNO_3 solution. Grain shape, crystal direction, and phase composition of the samples were analyzed by EBSD.

[1] UNIVERSITY OF ULSAN, SCHOOL OF MATERIALS SCIENCE & ENGINEERING, ULSAN, REPUBLIC OF KOREA
[2] KOREA INSTITUTE OF INDUSTRIAL TECHNOLOGY, INCHEON, REPUBLIC OF KOREA
[3] DAISHINKANGUP CO., LTD, ULSAN, REPUBLIC OF KOREA

* Corresponding author: jckimpml@ulsan.ac.kr

TABLE 1

Conditions used to synthesize samples in this study

Samples	Laser Power (W)	Laser Speed (mm/s)	Layer Thickness (µm)	Spot Size (µm)	Hatch Distance (µm)	Pattern
A1	150	860	30	70	200	Chess board
A2	160	860				
B1	150	1000				
B2	160	1000				

3. Results and discussion

Characteristics of the commercial MA6000 powder and the modified ODS Ni-based superalloy powders manufactured by the PGHA process are given in TABLE 2. The composition of the as-prepared powders were confirmed through EDX-XRF analysis. Elementals, Fe, and Mn were found in the ODS Ni-based superalloy. Fe and Mn were not present in the commercially available MA6000 sample. The Y content of 2.55 wt.% in the ODS Ni-super alloys was higher than the Y content of 1.10 wt.% in the commercial MA 6000 alloy.

SEM images of ODS Ni-based superalloy powders are shown in Fig. 1 The shape of the particles was mostly spherical with some satellites present on the surfaces of the micron-sized particles. This powder shape is suitable for the L-PBF process. For powder #1, however, the fine particles had low flowabil-

TABLE 2

Composition of ODS Ni-based superalloys and commercial MA6000 alloy manufactured by a gas hybrid atomization process

Element	Ni	Cr	Al	W	Ti	Mo	Ta	Zr	Y	Fe	Mn
MA6000 alloy	Balance	15.00	4.50	4.00	2.50	2.00	2.00	0.15	1.10	—	—
ODS Ni-super alloys	Balance	17.09	3.02	3.91	3.23	2.90	2.03	0.38	2.55	0.07	0.98

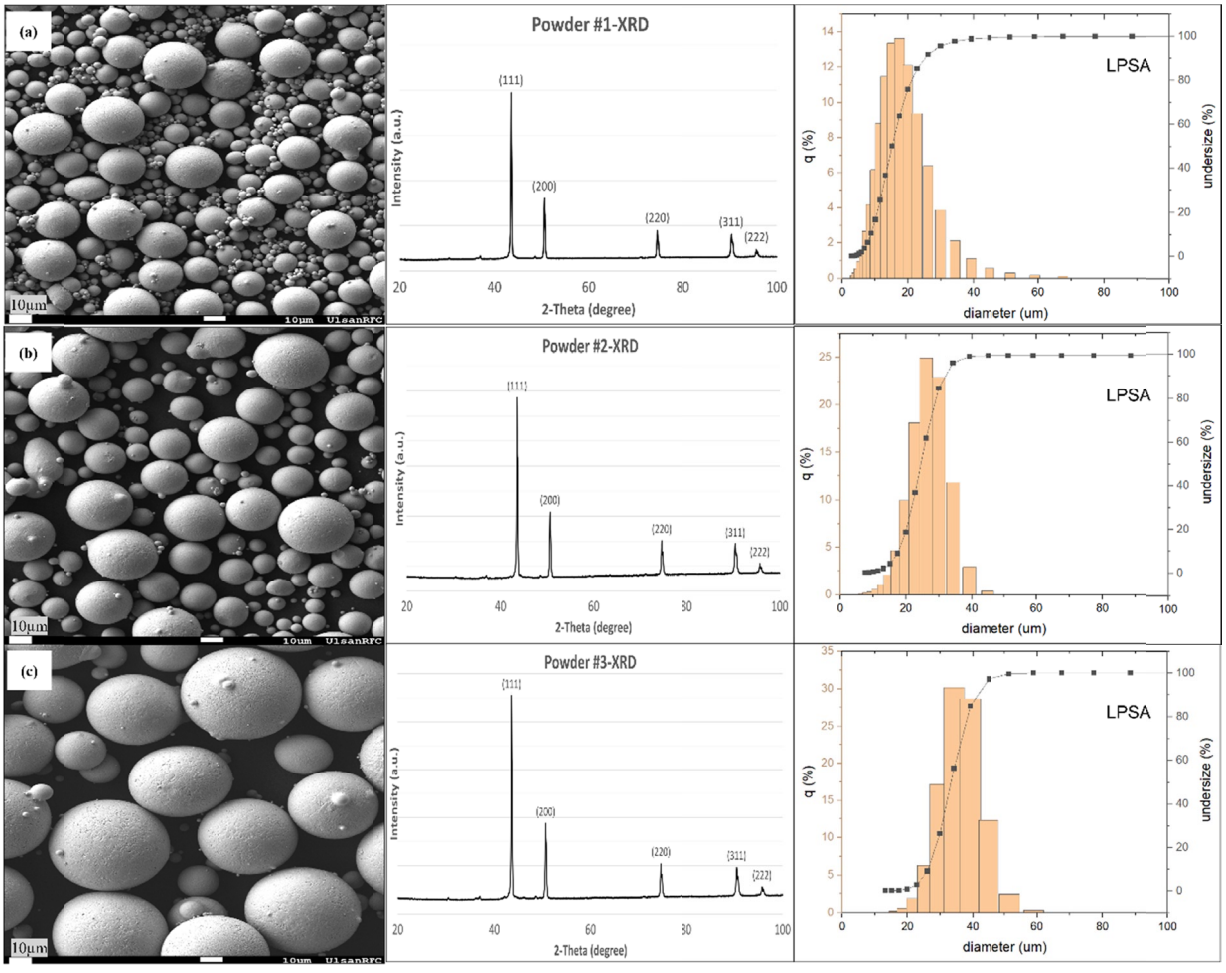

Fig. 1. LPSA, XRD, and SEM images of modified ODS Ni-based superalloy powders: (a) powder #1, (b) powder #2, (C) powder #3

ity making them unsuitable for L-PBF. Unlike ODS Ni-based superalloy powder #1, ODS Ni-based superalloys #2 and #3 powder had appropriate flowability. Thus, they were used in the L-PBF process.

SEM images and EDS analyses of the samples treated by L-PBF are shown in Fig. 2. Microdendrites were observed in each specimen and insoluble powders (indicated by the blue arrows) were unexpectedly observed in some areas on SEM images [5-8]. EDS analysis was performed to determine what these insoluble powders were. These insoluble powders contained Ta, Al, Si, and Y [8,9] and the content of the following elements was higher than that of the initial powders: Ni, Cr, and Ta [9,10].

EBSD analysis results for the L-PBF treated samples are shown in Fig. 3. Examination of the inverse pole figure (IPF) map of each specimen revealed that crystals grew in the <001>, <101>, and <111> directions depending on build direction [11]. A microstructure that hindered crystal growth according to build direction was present in the #2 ODS Ni-based superalloy (see

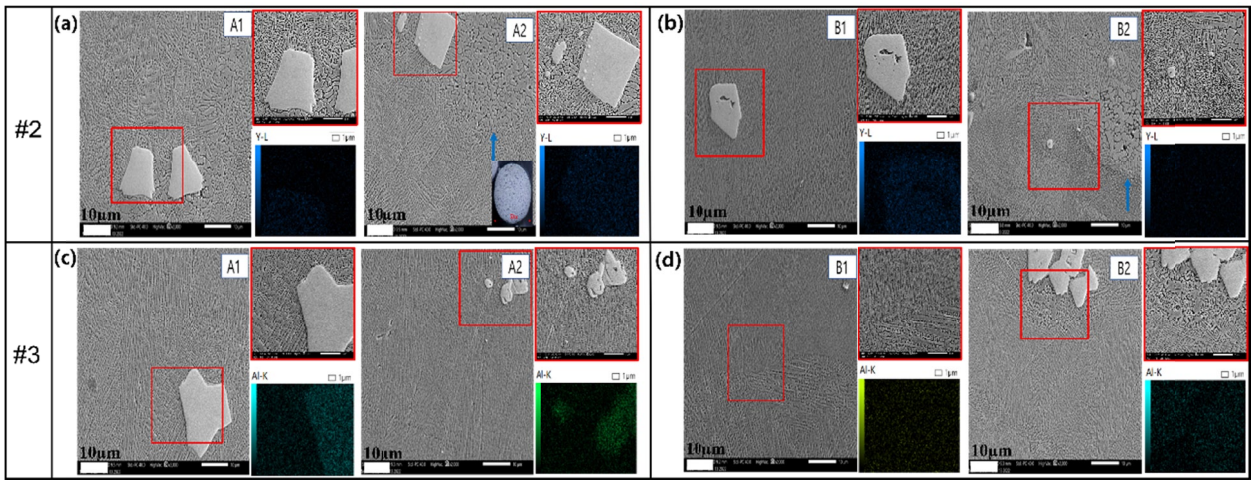

Fig. 2. SEM images and EDS results of L-PBF treated modified ODS Ni-based superalloys: (a-b) Specimens of ODS Ni-based superalloy powder #2. (a) A1, A2, (b) B1, B2, (c-d) specimens of ODS Ni-based superalloy powder #3. (c) A1, A2, (d) B1, B2

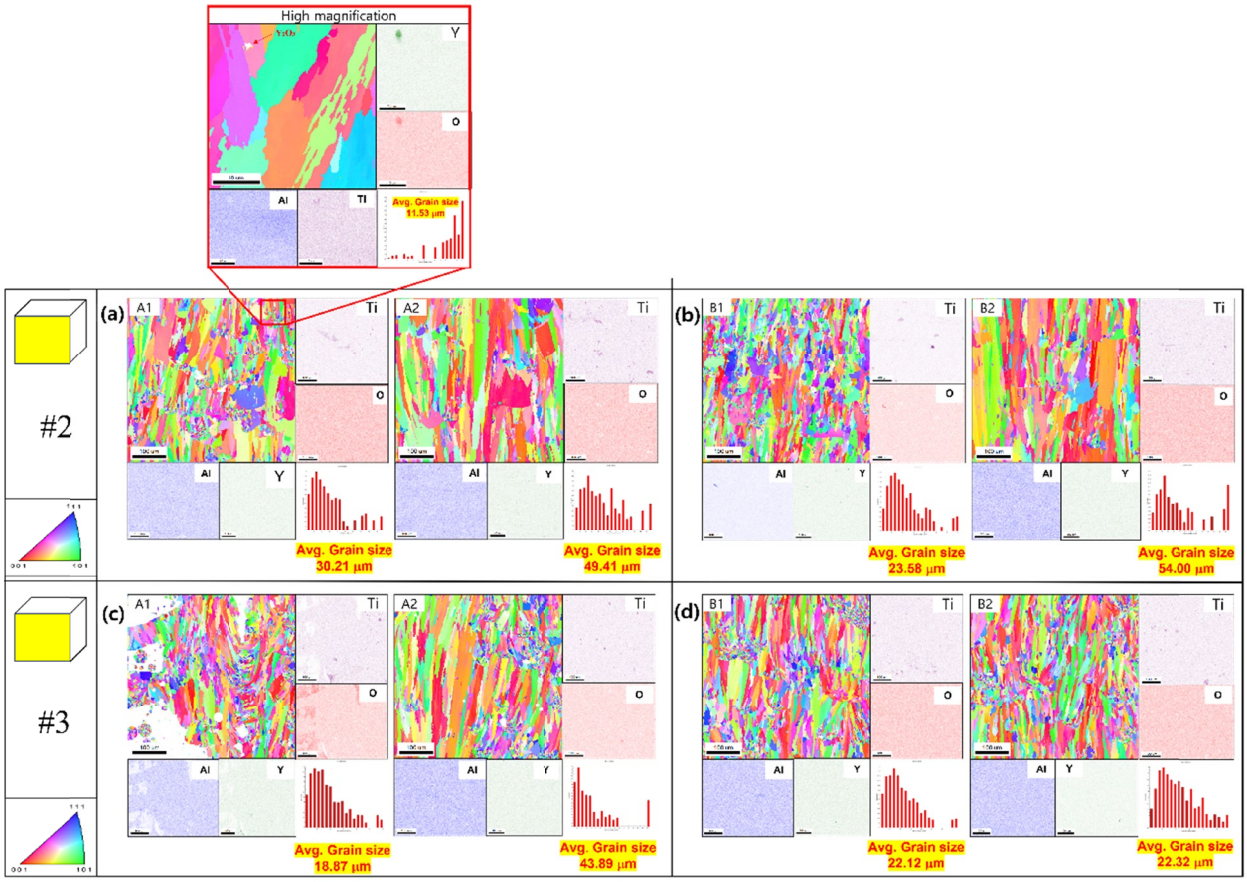

Fig. 3. EBSD data for modified ODS Ni-based superalloy samples: (a-b) specimens of ODS Ni-based superalloy powder #2, (c-d) specimens of ODS Ni-based superalloy powder #3. (high magnification: Y_2O_3 particles present in the A1 specimen)

Fig. 3) [11,12]. We confirmed that Ti was segregated in this superalloy and fine cracks were observed. When the powder #2 ODS Ni-based superalloy was viewed at higher magnification, Y_2O_3 (indicated by the arrow) was clearly seen near the grain boundaries [12,13] as shown in Fig. 3(a), Fig. 3(c), and Fig. 3(d) of ODS Ni-based superalloy #3 samples were like the results of (a) and (b) of powder #2, respectively. Cracks were observed for the L-PBF treated ODS Ni-based superalloy powder #3, and Ti intermetallic precipitates were observed in the grain boundaries of dendrites [12-15]. Micro Vickers hardness measurements were carried out to assess the mechanical properties of the specimens. The specimens of #2 powder exhibited hardness values of 395.6 HV, 352.5 HV, 405.7 HV, and 376.7 HV, while the specimens of #3 powder showed hardness values of 415.6 HV, 381.3 HV, 400.2 HV, and 425.2 HV.

4. Conclusions

The applicability of the 3D printing L-PBF process for creating modified ODS-Ni superalloy powders was investigated. Powders were generated using the PGHA process and the composition of the powders was studied by EDS-XRF. We confirmed that Fe, Mn, and Y_2O_3 were present in ODS-Ni superalloy powders but not commercial MA6000 powder. Three powder samples of ODS Ni-based super-alloys were studied: powder #1 (<25 μm), #2 (25 ~ 45 μm), and #3 (45 ~ 60 μm). Powders #2 and #3 were suitable for the L-PBF process. SEM and EBSD revealed microdendrites and Y_2O_3 oxides in the grains regardless of powder size. Ti intermetallic precipitates were also found in grain boundaries. These oxides and precipitates hindered crystal growth during PBF laser building.

Acknowledgments

This work was supported by the Ministry of Trade, Industry & Energy (MOTIE, Korea) under Industrial Technology Innovation Program No. 20017647, "Development of oxide dispersion strengthened superalloy materials and manufacturing technology for hypersonic engines."

This results was supported by "Regional Innovation Strategy (RIS)" through the National Research Foundation of Korea(NRF) funded by the Ministry of Education(MOE)(2021RIS-003)

REFERENCES

[1] Lin Zhang, Xuanhui Qu, Mingli Qin, Rafi-ud-din, Xinbo He, Ye Liu, Materials Chemistry and Physics **136**, 371-378 (2012).

[2] I.S. Kim, B.Y. Choi, Metals and Materials International **8**, 265-270 (2002).

[3] A.O.F. Hayama, H.R.Z. Sandim, J.F.C. Lins, M.F. Hupalo, A.F. Padilha, Materials Science and Engineering A **371**, 198-209 (2004).

[4] Ruifeng Xu, Zhaowen Geng, Yiyou Wu, Chao Chen, Mang Ni, Dan Li, Taomei Zhang, Hongtao Huang, Feng Liu, Ruidi Li, Kechao Zhou, Advanced Powder Materials **1**, 100056 (2022).

[5] Milad Ghayoor, Kijoon Lee, Yujuan He, Chih-hung Chang, Brian K. Paul, Somayeh Pasebani, Materials Science and Engineering A **788**, 139532 (2020).

[6] N.B. Dahotre, S. Harimkar, Laser Fabrication and Machining of Materials. Springer Science & Business Media, 2008.

[7] T. Guraya, S. Singamneni, Z. Chen, Journal of Alloys and Compounds **792**, 151-160 (2019).

[8] K.Q. Le, C. Tang, C.H. Wong, International Journal of Thermal Sciences **145**, 105992 (2019).

[9] V. Ramaswamy, P.R. Swann, D.R.F. West, Journal of the Less Common Metals **53**, 223-233 (1977).

[10] J. Park, Taesung, Jeoung Han Kim, Journal of Korean Powder Metallurgy Institute **25**, 327-330 (2018).

[11] De Luca, Anthony & Kenel, Christoph & Griffiths, Seth & Joglekar, Shreyas & Leinenbach, Christian & Dunand, David, Materials & Design **201**, 109531 (2021).

[12] Chao Wang, Xin Lin, Lilin Wang, Shuya Zhang, Weidong Huang, Materials Science and Engineering A **815**, 141317 (2021).

[13] Jovid U. Rakhmonov, Christoph Kenel, Anthony De Luca, Christian Leinenbach, David C. Dunand, Additive Manufacturing Letters **3**, 100069 (2022).

[14] Goo-Won Noh, Young-Do Kim, Kee-Ahn Lee, Hwi-Jun Kim, J. Korean Powder Metall. Inst. **27**, 8-13 (2020).

[15] Young-Kyun Kim, Seong-June Yoon, Jong-Kwan Park, Hwi-Jun Kim, Man-Sik Kong, Kee-Ahn Lee, J. Korean Powder Metall. Inst. **25**, 8-13 (2018).